Fast Boundary Detection: A Generalization and a New Algorithm

WERNER FREI, MEMBER, IEEE, AND CHUNG-CHING CHEN, STUDENT MEMBER, IEEE

Abstract—We study class of fast algorithms that extract object boundaries from digitized images. A set of orthogonal functions related to distinctive image features is presented, which allows efficient extraction of such boundary elements. The properties of these functions are used to define new criteria for edge detection and a sequential algorithm is presented. Results indicate considerable improvements over existing techniques, with a very moderate increase of computational cost.

Index Terms—Boundary detection, edge detection, feature extraction, image processing, orthogonal basis, sequential algorithm.

I. INTRODUCTION

AUTOMATIC scene analysis depends greatly on image segmentation into regions corresponding to individual objects. Assuming that these regions have some homogeneous characteristic, for example, luminance, color, texture, etc., one segmentation technique is to detect sharp transitions called edges, which tend to outline the desired boundaries. The opposite alternative is to "grow" regions by connecting small adjacent areas of similar characteristics. Of interest here is the detection of edges that separate regions of different constant luminances, and lines which can be regarded as a degenerate pair of edges. This operation requires the examination of several picture elements within contiguous or overlapping subareas of the image, followed by a decision as to whether an edge or a line segment is present or not within each subarea. The segments can be characterized by variables such as amplitude, orientation, position within the subarea, etc., and possibly a measure of confidence.

Upon examination of the whole picture, the object boundaries are constructed by connecting the edge and line elements detected previously. This operation can be directed by simple syntactic rules, for example connect neighbor edge elements that line up approximately, and delete isolated or parallel elements.

Some of the difficulties of edge detection are caused by noise, but much more so by the fact that visually distinct edges sometimes cannot be discriminated within a small image subarea or, conversely, that what appears to be an edge within the subarea could belong to a homogeneously textured domain of the picture. Increasing the size of the

subarea could apparently solve the problem, but is limited by computational cost and the complexity of large segment description.

It is generally recognized that boundary detection is therefore best done by the combination of a relatively simple edge and/or line segment detector, followed by algorithms that thin and link the segments obtained into continuous boundaries. Several fast numerical techniques for luminance edge extraction have been published, for example, Robert's "gradient" [1], Kirsch's [2], Sobel's [3], Prewitt's [4], Robinson's [5], and the so-called "smoothed gradient" [6] operators. Comparison of the above algorithms reveals similarities that suggest underlying general principles. From these we develop a set of orthogonal functions which are closely related to distinctive image features. The properties of these functions suggest ways to minimize the amount of computations as well as an improved decision criterion. A sequential algorithm is then presented and compared with several known techniques. Considerable improvements are obtained in terms of boundary "thickness," sensitivity to faint edges, insensitivity to smooth luminance gradients as well as variations of scene illumination.

This work is an extension of a previous study [7] at the Image Processing Institute of the University of Southern California.

II. DEFINITIONS

The problem of boundary element detection can be formulated as follows: given a set of n^2 luminance samples from an image subarea, determine whether the subarea contains a boundary element between two regions of different homogeneous luminances (edge). It may also be of interest to determine whether the area contains a line or a pair of degenerate edges enclosing an object too thin to be resolved. To this end, we define the following models of "ideal" boundary elements.

Consider an image subarea A of size $n \times n$ sampling intervals [Fig. 1(a)]. In the continuous image domain, we define an "ideal edge element" as a straight boundary, passing through the center of A, and which separates two regions of different, constant luminances $\bar{b}_1$ and $\bar{b}_2$. Adopting the convention $\bar{b}_1 > \bar{b}_2$, the direction φ_e of the edge element is uniquely determined with respect to any arbitrary, fixed direction [Fig. 1(b)]. The ideal edge element is characterized by its "magnitude" = $|\bar{b}_1 - \bar{b}_2|$ and orientation φ_e, $0 \le \varphi_e < 2\pi$.

Next we define an "ideal line element" (in the continuous image domain) as a straight strip of width approximately equal to one sampling interval, passing through the
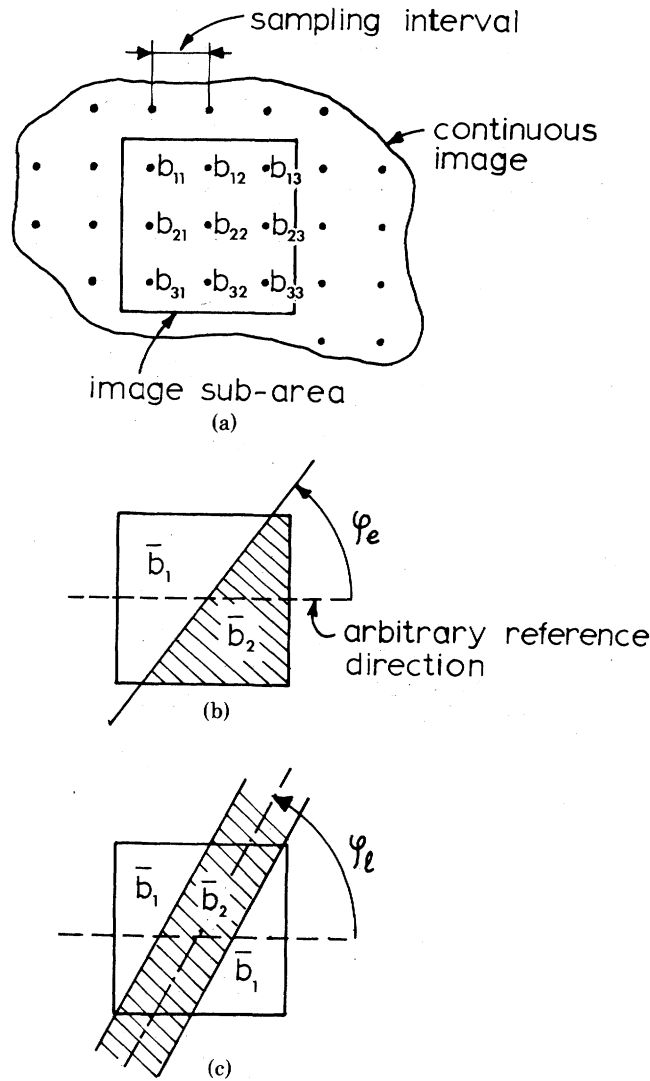
Fig. 1(a)   Definition of image subarea with components of subarea vector shown for the 3 × 3 pixel case; (b) definition of ideal edge element; (c) definition of ideal line element.

center of A, and of different luminance $\bar{b}_1$ than its surrounding $\bar{b}_2$ [Fig. 1(c)]. The ideal line element is characterized by its "magnitude" = $|\bar{b}_1 - \bar{b}_2|$, its orientation φ_l, $0 \leqq \varphi_l < \pi$ and polarity sgn $(\bar{b}_1 - \bar{b}_2)$.

Finally, an "ideal point" is defined as a point of brightness $\bar{b}_1$ different than a constant brightness $\bar{b}_2$ of the surround. The ideal point is characterized by its "magnitude" = $|\bar{b}_1 - \bar{b}_2|$ and polarity sgn $(\bar{b}_1 - \bar{b}_2)$.

For the discrete case, we define the following notation. Consider the set of n^2 luminance samples b_{ij} of the image subarea as an element of an n^2-dimensional vector space $\mathcal{B}$. The elements of $\mathcal{B}$ can be represented by a matrix B or a column vector $\boldsymbol{b}$, for example ($n = 3$)

$$B = \begin{bmatrix} b_{11} & b_{12} & b_{13} \\ b_{21} & b_{22} & b_{23} \\ b_{31} & b_{32} & b_{33} \end{bmatrix} \text{ or } \boldsymbol{b} = \begin{bmatrix} b_1 \\ b_2 \\ \vdots \\ b_{n^2} \end{bmatrix}.$$

Finally we define an inner (or dot) product $(\cdot, \cdot)$ on $\mathcal{B}$ as

$$(B,C) = \sum_{i=1}^{n} \sum_{j=1}^{n} b_{ij} c_{ij} \text{ or } (\boldsymbol{b}, \boldsymbol{c}) = \sum_{i=1}^{n^2} b_i c_i.$$

III. REVIEW OF PREVIOUS WORK

Previous fast edge detection algorithms (references cited) fall essentially into two categories.

1) Evaluate the maximum average gradient AG (or "smoothed gradient") present in each image subarea. The average is estimated in a direction perpendicular to the (unknown) edge element orientation and the maximum is approximately obtained by

$$AG \approx [(B,W_1)^2 + (B,W_2)^2]^{1/2} \tag{1}$$

where B is the vector of luminance samples and W_1, W_2 are weighting functions shown in Fig. 2(a)–(c) [1], [3], [6]. When the average gradient exceeds an arbitrary threshold, the image subarea is considered to contain an edge ele-
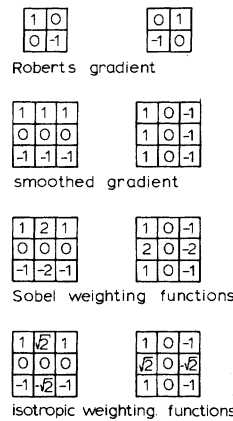
Fig. 2. Weighting functions for edge detection ([1], [6], [3], respectively, see text).
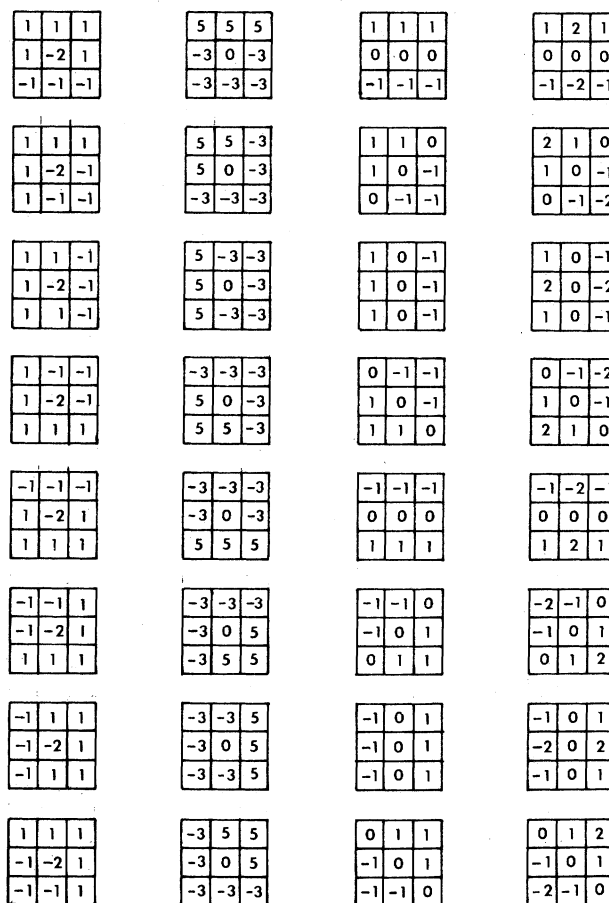

Fig. 3. "Templates" or "masks" for edge detection ([4], [2], [5], respectively).

ment. Orientation is then obtained approximately as

$$\varphi = \arctan\left[(B,W_1)/(B,W_2)\right].$$

In order to simplify computations, the sum of squares of (1) is sometimes replaced by a sum of absolute values. It is pointed out that the above measures are not isotropic, e.g., certain edge orientations are favored over other ones [5]. A pair of isotropic weighting functions is shown in Fig. 2(d).

2) The second approach is to form inner products of the luminance vector B with a set of discrete edge templates or masks T_i of different orientations as shown in Fig. 3(a)–(d) (see [2], [4], [5]), and retain the largest value

$$\max\{(B,T_i)\}.$$

When this value exceeds an arbitrary threshold, the subarea B is considered to contain an edge element. The direction is approximately equal ($\pm\pi/4$) to the orientation of the template giving the largest inner product.
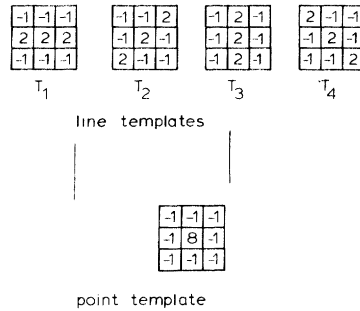
This second concept can be immediately extended to

line templates

point template

Fig. 4.   "Templates" or "masks" for (a) line detection; (b) point detection.

line and point detection with the template vectors shown in Fig. 4(a) and (b).

IV. IMPROVED DECISION STRATEGY

All algorithms discussed in the previous section can be interpreted as thresholding the magnitudes of the projections of the subarea vector B onto particular subspaces of $\mathcal{B}$. In the average gradient approach, we have one subspace of dimension two (spanned by W_1 and W_2), whereas in the template matching case, four (eight in [2] and [4]) subspaces of dimension one occur (the eight vectors of [5] are pairwise linearly dependent), spanned by the vectors T_i of Fig. 3.

We now propose an improved decision rule and ways to implement it economically. With the definitions of Section II, the problem of boundary element detection can be formulated as follows: determine how well a vector B of samples from an image subarea "fits" an ideal boundary element, not knowing its orientation a priori.

Suppose the existence of an "edge" subspace in $\mathcal{B}$ (as spanned for example by one of the template or mask sets of Fig. 3). Find a set of e orthogonal "edge" basis vectors $[T_1, \cdots, T_e]$ spanning that edge subspace, and expand the set with $n^2 - e$ "nonedge" basis vectors to span $\mathcal{B}$. Now consider the angle (in n^2-space) between B and its projection onto the edge subspace

$$\theta = \arccos \left[\sum_{i=1}^{e} (B, T_i)^2 \middle/ \sum_{j=1}^{n^2} (B, T_j)^2 \right]^{1/2}.$$

The larger $\theta (0 \leq \theta \leq \pi)$, the poorer the fit between B and an element of the edge subspace.

The decision strategy proposed is to classify image subareas as containing an edge element if θ is small. This can be done easily by thresholding the value of

$$\sum_{i=1}^{e} (B, T_i)^2 / (B, B) \tag{2}$$

which is an even function of θ, and is maximum for $\theta = 0$.

Fig. 5 depicts the effect of this new decision criterion, as compared to the traditional threshold techniques. Two subarea vectors B_1 and B_2 are shown, projected onto the "edge" and "nonedge" subspaces, respectively. Clearly, B_1 poorly fits an ideal edge element, because its projection onto the "nonedge" subspace is large. B_1 is rejected by our

criterion, whereas it is classified as an edge element by a conventional threshold decision. Conversely, B_2 is a good fit to the ideal edge element. It is classified as such by the θ-criterion, but rejected by the conventional decision rule. The same strategy can be employed to detect line elements and points as well, assuming that we have an orthogonal basis for "line" or "point" subspaces in $\mathcal{B}$.

It is pointed out that the measurement of (2) is invariant to scene illumination. It effectively extracts the reflection properties of object boundaries, providing that the illumination is constant over the subarea (sharp shadows are detected as edges!). This is easy to verify by substituting the luminances b_{ij} in (2) with $r_{ij} \cdot I$. The variables r_{ij} are scene reflectance values and I the illumination which cancels out in that equation.

V. ORTHOGONAL FEATURE BASIS

We now seek an appropriate basis for $\mathcal{B}$. Because the templates of Figs. 3(c) and 4(a) represent samples of ideal edge and line elements positioned in eight equidistant orientations, we assume "edge" and "line" subspaces of $\mathcal{B}$ spanned by these vectors. Of all possible orthogonal bases for these subspaces, we choose the one shown in Fig. 6, because of the following properties: 1) the first pair of basis vectors W_1 and W_2 represents the isotropic smoothed gradient weighting function. This pair, taken together with the second pair spans the above "edge" subspace. 2) The second pair of basis vectors W_3 and W_4 has a distinctive higher order aspect (three zero crossings instead of one) and will be shown to contribute little to the magnitude of the edge subspace component. 3) The "line" vectors were decomposed into a pair of vectors W_5, W_6 with directional preference and a pair W_7, W_8 without directional preference. Note that the point basis vector of Fig. 4(b) is equal to the sum of the latter pair, which, incidentally, span all possible discrete realizations of the discrete Laplacian [7]. Finally, the vector W_9 was added to complete the basis. Observe that linear combinations of each pair of vectors produce similar distinctive patterns, which we call "average gradient," "ripple," "line," and "Laplacian," respectively.

Figs. 7 and 8 illustrate the above discussions. An original image of size 256×256 pixels was projected onto each one of the nine orthogonal basis vectors of Fig. 6. Since the projections are bipolar, a constant value was added for
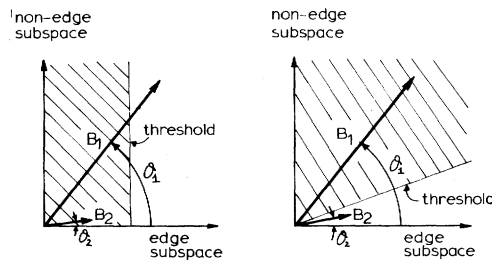
Fig. 5.   Graphical comparison of (a) conventional and (b) new boundary classification rule (see text).
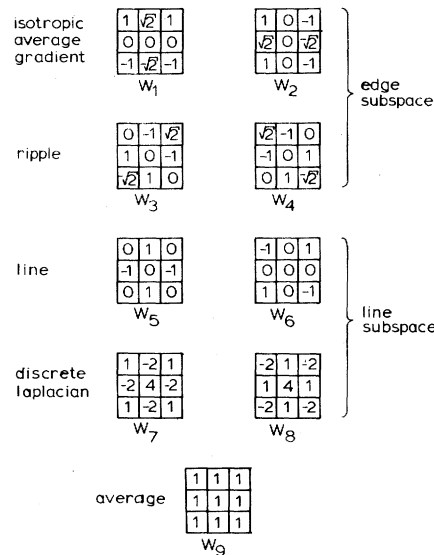

Fig. 6.   Orthogonal set of "feature" basis vectors.

display, and the images were scaled for better visibility. Fig. 8 shows the magnitudes of the projections onto the four-dimensional edge and line subspaces. The complementary nature of these subspaces is clearly visible and can be attributed to the fact that the edge basis vectors are odd with respect to one axis of symmetry whereas the line basis vectors are even [see Figs. 3(c) and 4(a)]. This observation appears to add significance to the new decision strategy proposed.

In order to reduce computations, it would be desirable to reduce the dimension of the feature subspaces. Fig. 9 shows the magnitudes of the projections onto the "average gradient," "ripple," "line," and "point," respectively. While the last pair of projections appear similar (any line is composed of points!), the "average gradient" and "ripple" projections are quite different. It is easy to see that the "ripple" subspace contributes little to the "edge" subspace [compare Figs. 8(a) and 9(a)] and may be ignored to save computations.

Next the effects of the new feature measure proposed are depicted in Fig. 10(a)–(d), which were obtained as follows:

$$\sum_{i=k}^{k+1} (B,T_i)^2/(B - \overline{B}, B - \overline{B})$$

with $k = 1, 3, 5, 7$ and $\overline{B} = (B,T_9)$. ($\overline{B}$ was subtracted from B in the denominator to improve the visibility of the image structures obtained.)

Fig. 10 strikingly reveals the advantages and disadvantages of the new measure. On one hand, very fine structural detail has been made visible, but unfortunately, smooth luminance gradients are now likely to be erroneously classified as broad clusters of "edge" points. This undesirable effect follows from the impossibility to determine whether a luminance gradient extends beyond the boundaries of the subarea examined. One solution would be to increase the size of the subareas, but this is undesirable from a computational point of view. On the other hand, it is recalled that the desired boundaries are "line" features in the edge measurement "picture" obtained from (2), and visualized in Fig. 10(a). These line elements can be detected by projecting the edge measurement "picture" onto the "line" subspace of $\mathcal{B}$, and then applying the decision rule of Fig. 5 to that subspace. In images containing
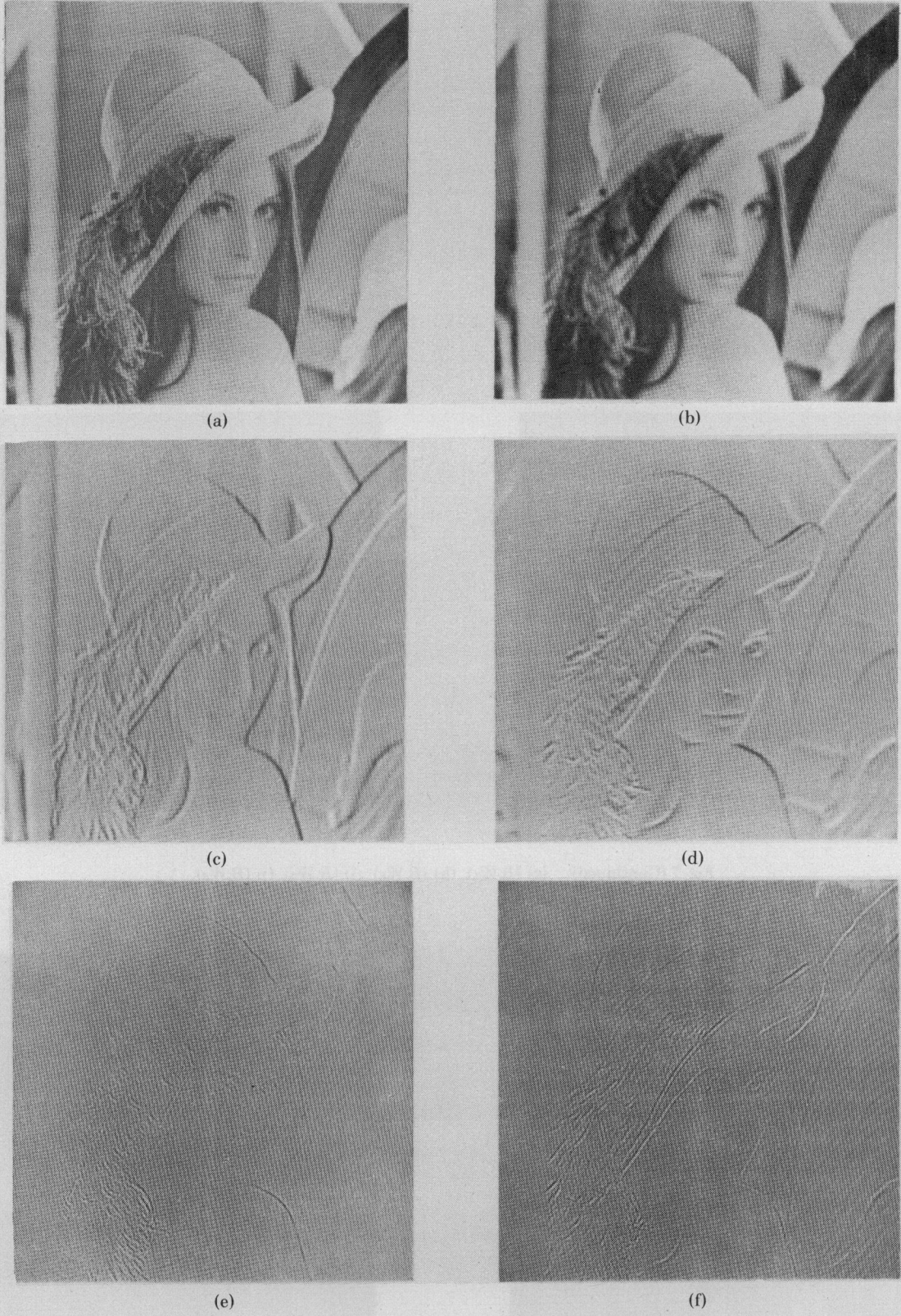
Fig. 7. Projections of image onto orthogonal basis vectors. (a) Original image. (b) (B,W). (c) (B,W_1). (d) (BW_2). (e) (B,W_3). (f) (B,W_4).
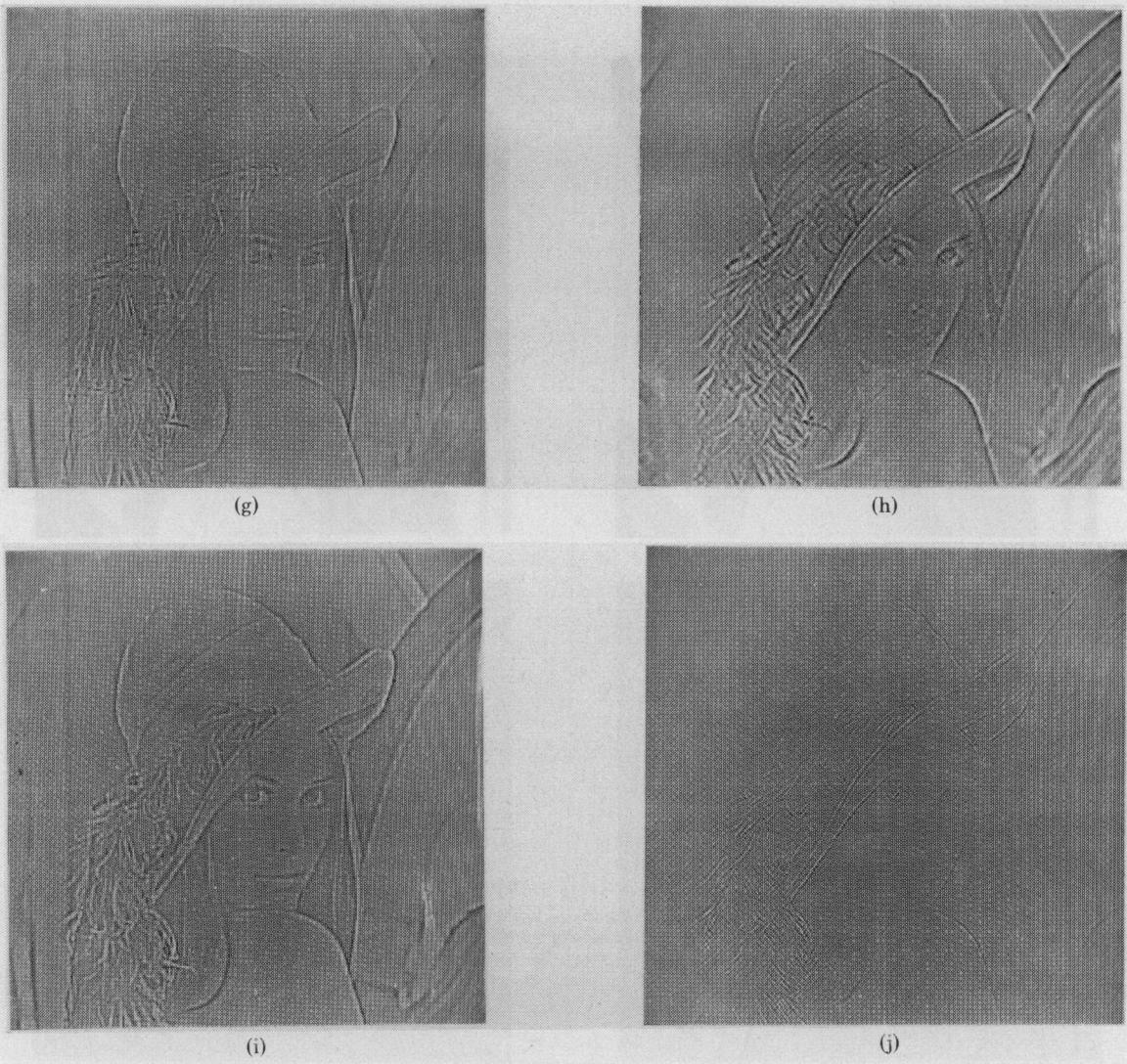
(g)

(h)

(i)

(j)

Fig. 7 (Continued).   (g) (B, W_5). (h) (B, W_6). (i) (B, W_7). (j) (B, W_8).
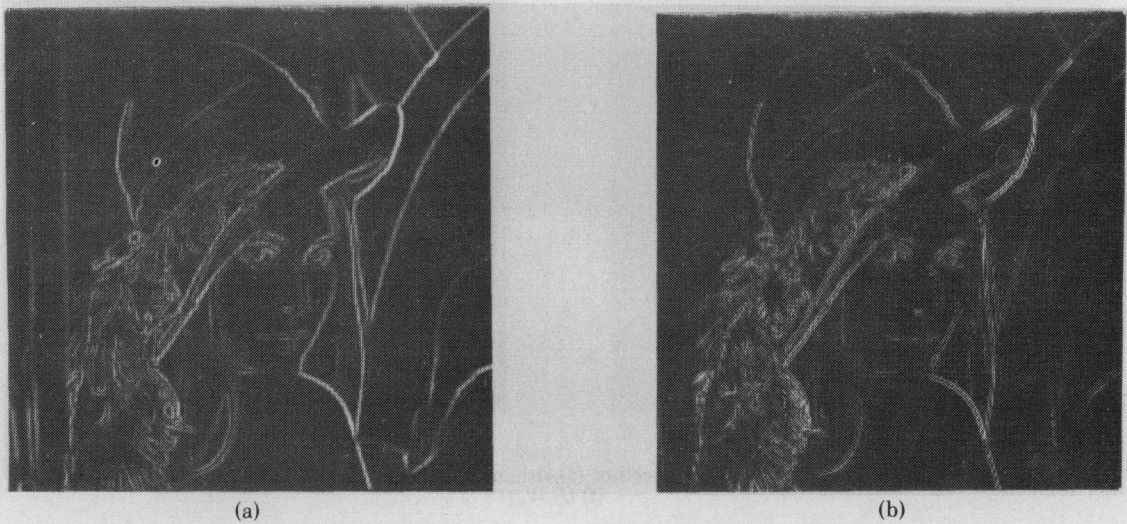

(a)

(b)

Fig. 8.   Magnitude of projections onto edge and line subspaces. (a) $\Sigma_{i=1}^{4} (B, W_i)^2)^{1/2}$. (b) $\Sigma_{i=5}^{8} (B, W_j)^2)^{1/2}$.
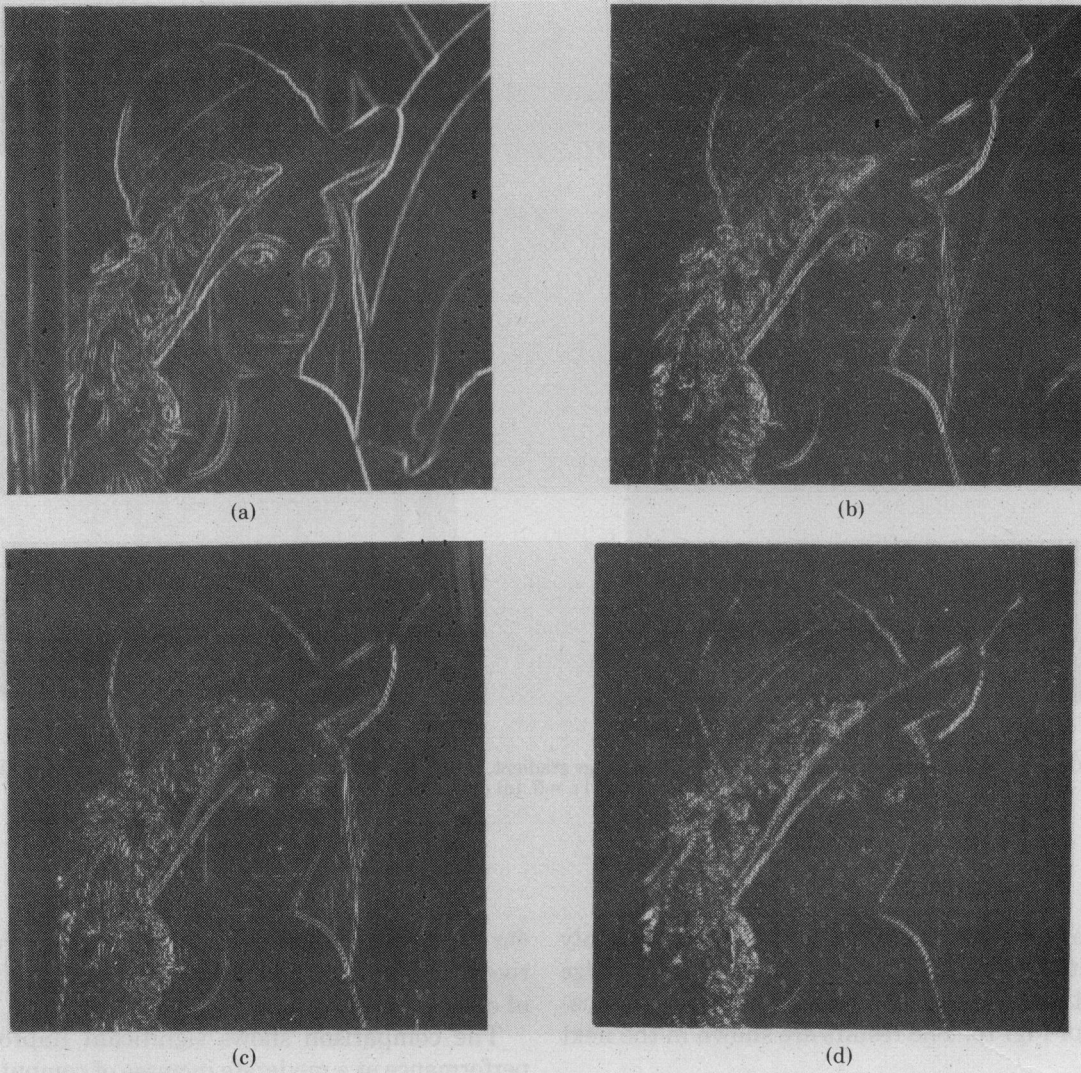
Fig. 9. Magnitude of projections onto "average gradient," "ripple," "line," and "Laplacian" subspaces, respectively. (a) $((B,W_1)^2 + (B,W_2)^2)^{1/2}$ (averaged gradient). (b) $((B,W_3)^2 + (B,W_4)^2)^{1/2}$ (ripple). (c) $((B,W_5)^2 + (B,W_6)^2)^{1/2}$ (line). (d) $((B,W_7)^2 + (B,W_8)^2)^{1/2}$ (Laplacian).
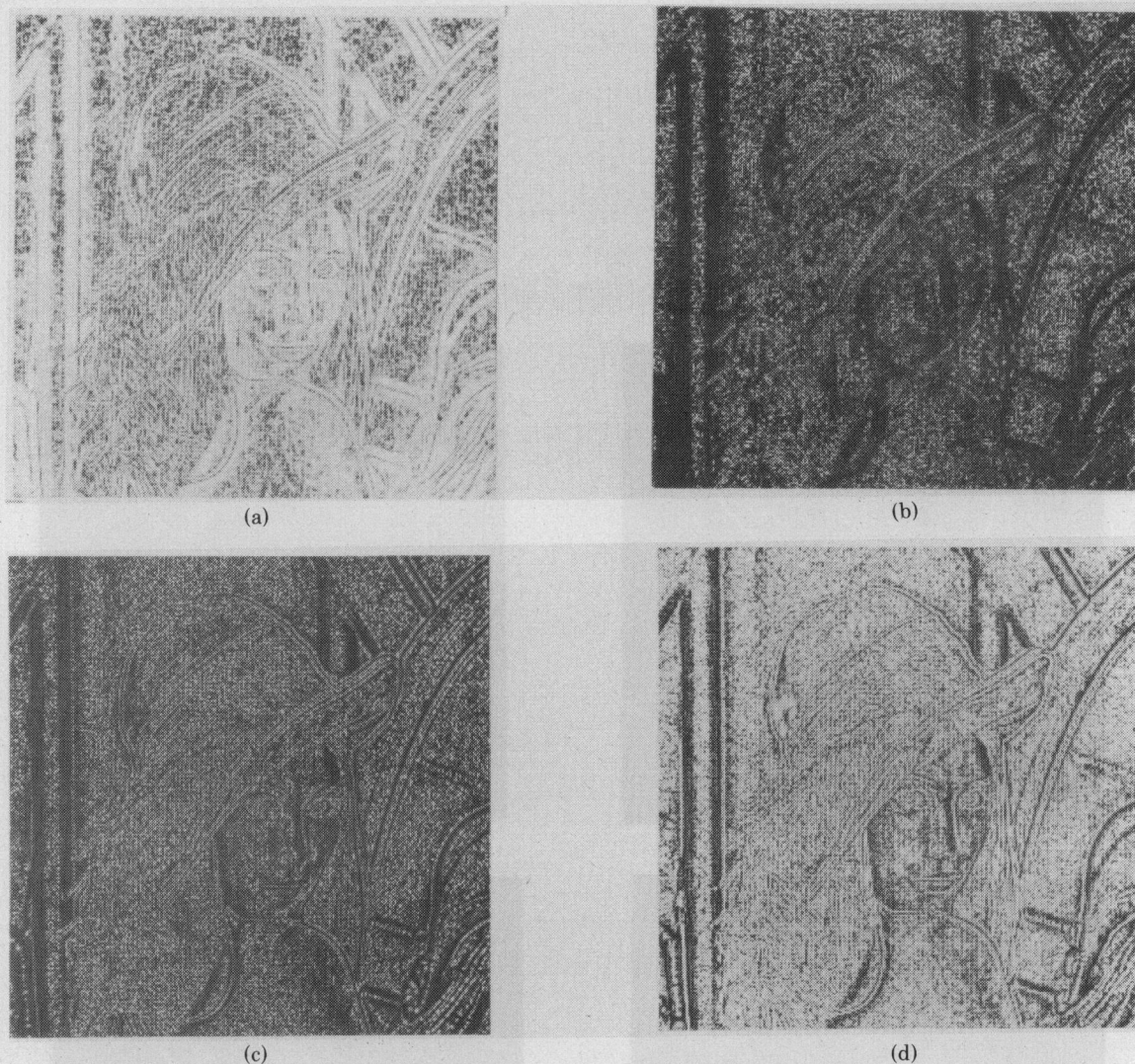
Fig. 10.   Normalized magnitude of projections onto "average gradient," "ripple," "line," and "Laplacian" subspaces, respectively.
(a) $i = 1$. (b) $i = 3$. (c) $i = 5$. (d) $i = 7$.

little noise however, it was found that it suffices to apply "point" detection [using the vector of Fig. 4(b)] to the edge measurement "picture," to eliminate the unwanted clustering effect of Fig. 10. The results are shown in the next section.

VI. COMPARISONS

In this section we compare the new algorithm proposed with the Kirsch and Sobel operators [2], [3]. In order to visualize the improvements obtained, the three algorithms were run on the same original image and thresholds adjusted to obtain approximately the same number of edge points. Fig. 11 shows this comparison which clearly reveals the following improvements:

1) much more subtle edges are detected,

2) "strong" edges are detected as thinner lines (minimizing the need for "thinning" operations),

3) edges in dark areas of the image are more likely to be detected.

On the negative side, we note a slightly increased sensitivity to noise. Table I shows a comparison of the number of computations required.

The comparison shows significant improvements of performance at a moderate increase of computational cost. A similar algorithm can be used for line detection in images that contain such features. As Fig. 8 shows, lines tend to be detected on both sides of edges and vice versa. This property could be exploited to further refine the algorithm but was not explored in detail here.

ACKNOWLEDGMENT

Fig. 11.   Comparison of Kirsch, Sobel, and proposed edge detection algorithms. Isolated points were deleted as indicated.

TABLE I
Number of Computations per Edge Point

|	Sobel	Kirsch	Proposed sequential Algorithm
Multiply or Divide	4	9	13
Add or Subtract	11	21	27
Compare	1	9	1

REFERENCES

[1] L. G. Roberts, "Machine perception of three-dimensional solids," in *Optical and Electro-Optical Information Processing,* J. T. Tippett *et al.,* eds. Cambridge, MA: MIT Press, 1965.

[2] R. Kirsch, "Computer determination of the constituent structure of biological images," *Comput. Biomed. Res.,* vol. 4, pp. 315–328, 1971.

[3] R. O. Duda and P. E. Hart, *Pattern Classification and Scene Analysis.* New York: Wiley, 1971.

[4] J. M. S. Prewitt, "Object enhancement and extraction," in *Picture Processing and Psychopictorics,* B. S. Lipkin and A. Rosenfeld, eds. New York: Academic Press, 1970, pp. 75–149.

[5] G. S. Robinson, "Detection and coding of edges using directional masks," Univ. of Southern California, Los Angeles, CA, USC-IPL Rep. 660, pp. 40–57, Mar. 1976.

[6] T. S. Huang, Purdue University, Lafayette, private communication, 1975.

[7] W. Frei, "A new class of edge and feature detection operators," Univ. of Southern California, Los Angeles, CA, USC-IPL Rep. 660, pp. 22–40, Mar. 1976.

[8] Z. Meiri, Bell Lab., private communication, Jan. 1976.

Werner Frei (S'70–M'74) received the B.S. degree in 1968 and the Ph.D. degree in 1972 in electrical engineering from the Federal Institute of Technology, Zurich, Switzerland.

He then became an Assistant Professor at the Department of Electrical Engineering, University of Southern California, Los Angeles, and member of the staff at the USC Image Processing Institute. There, his research was directed towards digital image coding and processing, as well as related phenomena of visual perception. In 1976, he joined the faculty of the USC Medical School, where he is in charge of the digital image analysis research effort pursued by the Medical Imaging Sciences Group of the Department of Radiology.
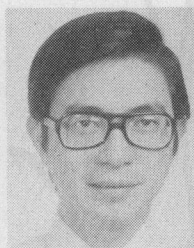
Chung-Ching Chen (S'74) was born in Taiwan, China on June 25, 1950. He received the B.S. degree in electrical engineering from the National Taiwan University, Taiwan, China, in 1972, and the M.S. degree from the University of Southern California, Los Angeles, in 1976.

From 1974 to 1975 he was a Teaching and Research Assistant in the Department of Electrical Engineering at USC. In 1975, he became a Research Assistant at the Image Processing Institute at USC, where he is currently engaged in picture processing and image understanding research.

Mr. Chen is a member of Sigma Xi.

A General Model for Memory Interference in Multiprocessors

CORNELIS H. HOOGENDOORN

Abstract—This paper presents a mathematical model for determining the extent of memory interference in multiprocessor systems. The model takes into account the numbers of processors and memory modules in the system and their relative service times, as well as the patterns of memory accesses made by the processors. The results predicted by the model are compared with simulation results and with results from other exact or approximate models, where these exist.

Index Terms—Analytic models, memory interference, multiprocessors, performance evaluation, simulation.

I. INTRODUCTION

IN a multiprocessor system main memory may consist of several memory modules, each of which can be accessed by all the processors in the system. A memory conflict occurs whenever two or more processors attempt to access the same memory module simultaneously. When a conflict occurs, all but one of the conflicting processors will be delayed. The overall effect of these conflicts, referred to as memory interference, is a decrease in the execution rate of the processors.

Factors that influence the extent of memory interference in a multiprocessor include the following.

1) The numbers of processors and memory modules.